remote sensing

MDPI

Article

A Full-Waveform Airborne Laser Scanning Metric Extraction Tool for Forest Structure Modelling. Do Scan Angle and Radiometric Correction Matter?

Pablo Crespo-Peremarch * and Luis A. Ruiz

Geo-Environmental Cartography and Remote Sensing Group (CGAT), Department of Cartographic Engineering, Geodesy and Photogrammetry, Universitat Politècnica de València, Camí de Vera s/n, 46022 València, Spain; laruiz@cgf.upv.es

* Correspondence: pabcrepe@cgf.upv.es

Received: 21 November 2019; Accepted: 13 January 2020; Published: 15 January 2020

Abstract: In the last decade, full-waveform airborne laser scanning (ALS_{FW}) has proven to be a promising tool for forestry applications. Compared to traditional discrete airborne laser scanning (ALS_D), it is capable of registering the complete signal going through the different vertical layers of the vegetation, allowing for a better characterization of the forest structure. However, there is a lack of ALS_{FW} software tools for taking greater advantage of these data. Additionally, most of the existing software tools do not include radiometric correction, which is essential for the use of ALS_{FW} data, since extracted metrics depend on radiometric values. This paper describes and presents a software tool named *WoLFeX* for clipping, radiometrically correcting, voxelizing the waves, and extracting object-oriented metrics from ALS_{FW} data. Moreover, extracted metrics can be used as input for generating either classification or regression models for forestry, ecology, and fire sciences applications. An example application of *WoLFeX* was carried out to test the influence of the relative radiometric correction and the acquisition scan angle (1) on the ALS_{FW} metric return waveform energy (RWE) values, and (2) on the estimation of three forest fuel variables (CFL: canopy fuel load, CH: canopy height, and CBH: canopy base height). Results show that radiometric differences in RWE values computed from different scan angle intervals (0°–5° and 15°–20°) were reduced, but not removed, when the relative radiometric correction was applied. Additionally, the estimation of height variables (i.e., CH and CBH) was not strongly influenced by the relative radiometric correction, while the model obtained for CFL improved from R^2 = 0.62 up to R^2 = 0.79 after applying the correction. These results show the significance of the relative radiometric correction for reducing radiometric differences measured from different scan angles and for modelling some stand-level forest fuel variables.

Keywords: LiDAR; software tool; processing tool; relative radiometric correction; forest fuel; understory vegetation

1. Introduction

Laser scanning has been used in the last several decades for a wide range of applications, such as climate change monitoring through biomass estimation [1,2], carbon sequestration [3,4] and wildlife protection [5,6]. Its potential is based on the registration of a dense 3D point cloud, which is time and cost efficient compared to traditional methods. The 3D point cloud provides geometric and spectral data, given by the XYZ coordinates and the intensity value, respectively. In forestry applications, laser scanning is capable of registering accurate data from the different vertical strata, providing complementary information to other remote sensing techniques for a better characterization of forest

structure [7]. Among laser scanning technology and within forestry applications, terrestrial laser scanning (TLS) registers a highly dense point cloud of the low and intermediate strata due to its proximity to the objects and ground position. Some of the applications of TLS are segmentation of the tree branching structure and estimation of the foliage biomass [8] and leaf area density at the voxel level [9]. On the other hand, discrete airborne laser scanning (ALS_D) can register larger areas, and it has been widely used to estimate some forest variables at stand- and individual-tree-level by tree segmentation approaches (e.g., [10,11]). Some of them are forest structure variables such as diameter at breast height (DBH) [12,13], basal area [14,15], stem volume [16,17], stem density [13–15], stand volume [18,19], fractional cover/gap fraction, and leaf area index (LAI) [20,21]; forest mass variables, such as biomass components [13,17,19]; and forest fuel variables, such as mean and dominant tree heights [18,22], canopy base height, canopy fuel load, and canopy bulk density [19,23]. Moreover, ALS_D data have also been used in combination with multispectral or hyperspectral images to classify tree species [24,25] and fuel types [24,26,27]. The forest fuel variables mentioned (i.e., canopy bulk density, canopy fuel load, canopy base height, and dominant tree height) describe the forest fuel load as well as the horizontal and vertical structure. These are key inputs for fire behavior models, since they describe amount of fuel and its vertical and horizontal continuity [28].

Among ALS technology, full-waveform ALS (ALS_{FW}) is a more complex data type capable of registering the entire signal emitted by the sensor as a pulse and backscattered from the different vertical layers and the ground [29]. This signal is represented as a waveform whose amplitude values vary along the elapsed time depending on the physical properties of the intercepted layers [30]. As a result, a continuous analysis of the forest vertical structure can be undertaken. Among other uses, ALS_{FW} data have also been used to estimate forest stand variables [31], forest structure and fuel models [30], to segment trees [32], and to classify tree species [33,34]. Hence, given that ALS_{FW} provides more information from the different vertical layers compared to ALS_D, it has a great potential to study the forest structure [31,35,36] and understory vegetation [37,38]. Since ALS_D and ALS_{FW} have different data structures (i.e., based on a point cloud and waveforms, respectively), new ALS_{FW} metrics have been proposed in the last decade to carry out the studies mentioned above. Most of the ALS_{FW} metrics proposed were originally created for large-footprint ALS_{FW} (i.e., diameter between 10 and 25 m) [39–42], and others were tested directly for small-footprint ALS_{FW} (i.e., diameter lower than 1 m) [38,43]. Although most of the metrics were created for large-footprint ALS_{FW}, they were also used in several studies extracted from small-footprint ALS_{FW}, obtaining promising results in characterizing and modelling forest structure [30,31,38,44].

An essential pre-processing step before generating ALS_{FW} metrics is the radiometric correction [45]. Radiometric correction or calibration is a widely used term in remote sensing imagery. The goal of this correction is to reduce errors in the acquired digital values of the pixels due to atmospheric or sensor factors [46]. This process is fundamental when dealing with images acquired from different sensors or on different days [47]. Additionally, radiometric correction may involve converting digital numbers to physical units [48]. This process is less extended for ALS data, but it is an essential step for ALS_{FW} due to the reliance between ALS_{FW} metrics and amplitude values [49]. The use of ALS_{FW} data without radiometric correction may lead to modified ALS_{FW} metrics, and consequently modified estimates of forest fuel variables. In this case, the goal of the radiometric correction is to provide amplitude values independent of the angle of incidence, range from the sensor to the target, as well as sensor and flight day atmospheric conditions. Attending to Briese et al. [50], there are two main types of radiometric correction of ALS_{FW}: (i) correcting radiometric differences between flight lines without auxiliary data (i.e., relative correction) or (ii) using a surface whose approximate reflectance values are known or using measured reflectance values from ground targets (i.e., absolute correction). The use of any of these corrections, which depends on the available data and the presence of well-known surfaces, has been pointed out by some authors as a relevant pre-processing step of ALS_{FW} data sets [49,51].

There are several processing tools available to retrieve ALS_D metrics, which are further used to predict forest fuel variables. Two well-known software tools are *FUSION/LDV* [52] and *LAStools* [53].

Additional libraries for processing ALS_D data are available in different programming languages (e.g., *lidR* in R as used by Roussel and Auty [54]; *laspy* in Python (http://laspy.readthedocs.io/en/latest/)), such that users can customize their own tool for specific needs. However, due to the complexity of the use of ALS_{FW} data and the non-standard level of its use and application, there is a very limited number of processing tools available for ALS_{FW} data, both at open and commercial levels. Researchers working on ALS_{FW} have developed their own tools for specific purposes, while others have made their tools available. Zhou and Popescu [55] developed an R package named *waveformlidar* to process and visualize ALS_{FW} data. This package allows for processing ALS_{FW} data through two different strategies: (i) by means of deconvolution or decomposition of waveforms, therefore providing ALS_D point clouds with more information (e.g., echo width); and (ii) generating dense point clouds from waveforms, self-named as "hyper point clouds". Furthermore, some commonly used ALS_{FW} metrics, including those proposed by Duong [41], may also be retrieved by voxelizing the hyper point clouds through the *waveformlidar* package. Miltiadou et al. [56] created another open source software tool to process ALS_{FW} and hyperspectral imagery data called *DASOS*. This tool visualizes a polygon representation from voxelized ALS_{FW} data and computes ALS_{FW} metrics at the voxel column level. Most of these metrics are related to height, distance between voxels, and number of empty/full voxels, except for the maximum and average intensity values of the voxel column. Another available tool for ALS_{FW} data processing is *OPALS* (Orientation and Processing of Airborne Laser Scanning data) [57]. This tool computes an ALS_{FW} decomposition, but not specific ALS_{FW} metrics from the whole waveform amplitudes. Apart from ALS_D, *LAStools* allows for the visualization of ALS_{FW} data through *PulseWaves* [58] by representing the trajectories of the pulses. Among the software tools mentioned, only *waveformlidar* and *OPALS* include the radiometric correction, with the relative radiometric correction being recently included in *OPALS* [51]. However, more tools are needed in order to cope with a wider range of metrics able to better characterize forest structure (e.g., understory vegetation metrics), as well as to offer a more straightforward approach for the radiometric correction of raw ALS_{FW} data.

In this paper, we present a new software tool named *WoLFeX* (Waveform Lidar for Forestry eXtraction) that compiles a set of methods to process and analyze ALS_{FW} data, including the extraction of most ALS_{FW} metrics as proposed in the literature, and new metrics focused on understory vegetation. These metrics are crucial for modelling forest fuel variables and forest structure. The tool also allows for the relative radiometric correction of the data, reducing the effect of the different angles of incidence and local altitude variations during the data acquisition process. In addition, we assessed the influence of the scan angle of ALS data acquisition and the application or not of a radiometric correction on (i) the extraction of an ALS_{FW} metric; and (ii) modelling three of the most relevant forest fuel variables—canopy fuel load (CFL), canopy height (CH), and canopy base height (CBH).

2. Full-Waveform ALS Data Processing

One of the most common methodologies proposed to process ALS_{FW} data to study and model the three-dimensional structure of forests is the one based on the voxelization and generation of pseudo-vertical waveforms [59]. The standard overall processing of ALS_{FW} to extract metrics is described in Figure 1.

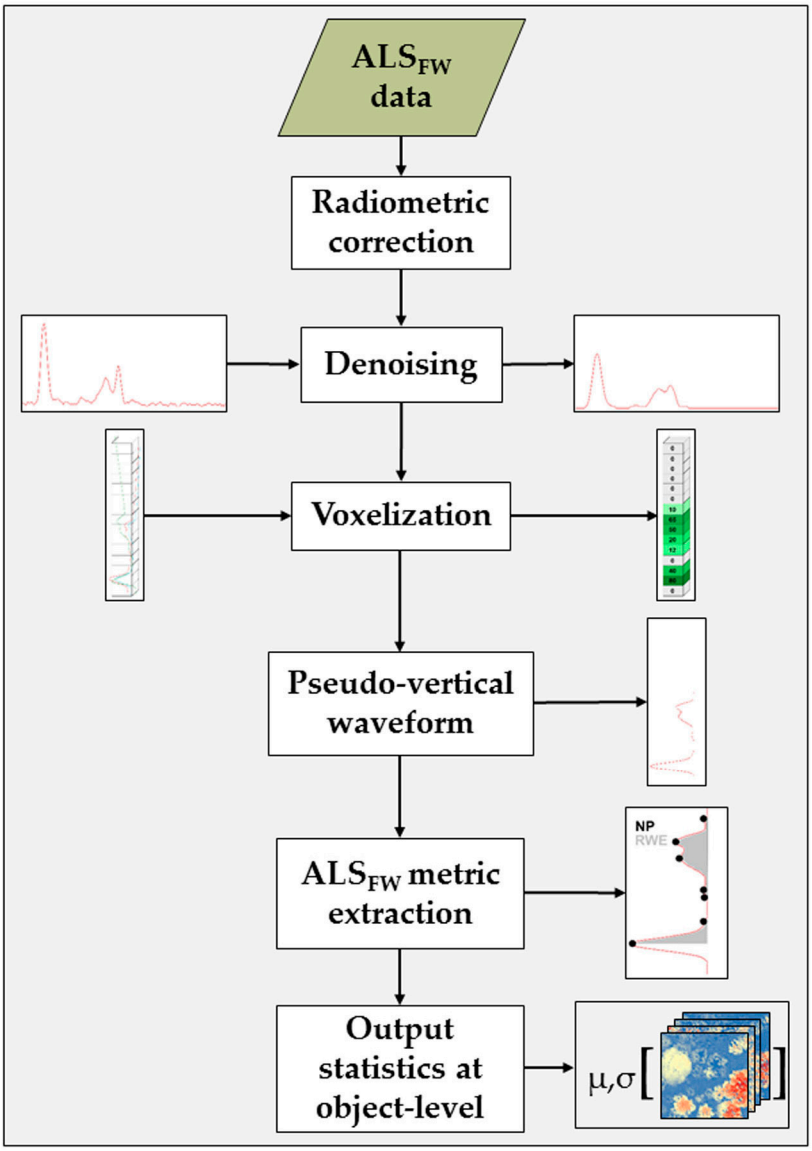

Figure 1. Overall process to extract full-waveform airborne laser scanning (ALS$_{FW}$) metrics.

2.1. Radiometric Correction

The first ALS$_{FW}$ processing step consists of the radiometric correction of the amplitude values contained in each waveform bin. This is especially critical for ALS$_{FW}$, since the metrics extracted to create the models are directly related to the amplitude values. Our approach is based on the use of the relative radiometric correction—a more straightforward method than the absolute one where no reference ground data are needed. The relative radiometric correction consists of correcting the amplitude values from differences in the angle of incidence and the distance from the sensor, due to different orientations of the sensor and flight lines, in order to reduce the influence of these parameters on the final radiometric values. Equation (1), described by Kashani et al. [60], considers the distance from the sensor to the registered object and the angle of incidence. The angle of incidence depends on the scan angle, the slope, and the aspect (Figure 2). Knowing these values, we are able to calculate the angle of incidence for those ALS$_{FW}$ returns corresponding to the ground. However, objects present on the ground (e.g., trees) do not follow the terrain slope. As an assumption, trees grow vertically, and their branches grow almost horizontally. Since it is unfeasible to know the real angle of incidence on tree leaves and branches without accurate external data (e.g., terrestrial laser scanning), for the

computation of the angle of incidence we assumed the terrain slope for ALS_{FW} ground returns, and a null slope (i.e., 0%) for the rest of ALS_{FW} returns (i.e., branch and leaf returns).

$$A_C = A \times \frac{{R_i}^n}{{R_{ref}}^n} \times \frac{1}{cos\alpha}, \quad (1)$$

where A_C is the corrected amplitude; A is the original amplitude; R_i is the range from the sensor to the ALS_{FW} return i; R_{ref} is the reference range, which is a constant value defined by the user to normalize R_i; α is the local angle of incidence, and n is the power of the range.

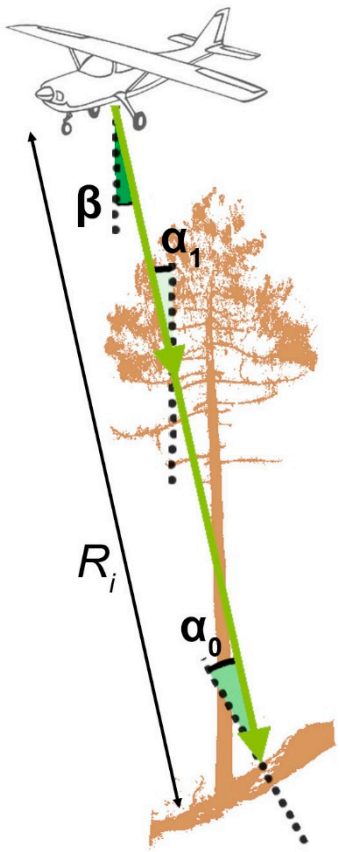

Figure 2. Relation between the angle of incidence at the ground (α_0) and at a branch (α_1), the scan angle (β), and the range from the sensor to ALS_{FW} return corresponding with the ground (R_i).

2.2. Denoising

After the radiometric correction, a denoising process is needed to remove the noise due to the system registration process. We followed the process described by Hermosilla et al. [59], consisting of first discarding noisy waveforms, and then removing noise from non-noisy waveforms. In this process, waveforms are tagged as noisy when all the amplitudes are below a threshold defined as the mean plus four times the standard deviation of the waveform amplitudes [61]. All these waveforms are removed, and only the rest of waveforms (i.e., non-noisy) are used for the next step. For the remaining waveforms, two denoising filters may be applied. First, noise, defined as 133% of the mode of the amplitudes, is subtracted from each amplitude value of the waveform. Then, a Gaussian filter is applied to eliminate the remaining noise.

2.3. Voxelization and Generation of Pseudo-Vertical Waveforms

The next step is the voxelization of ALS_{FW} data, which consists of computing amplitude statistics (i.e., maximum, mean, median, etc.) from all the waveforms crossing a voxel (i.e., a three-dimensional

pixel). As a result of this step, ALS_{FW} data are substantially reduced, and pseudo-vertical waveforms [59] are generated. Pseudo-vertical waveforms are obtained based on the amplitude values of every voxel column, correcting off-nadir waveforms. Pseudo-vertical waveforms allow for an easier metric extraction process.

2.4. ALS_{FW} Metric Extraction

Once pseudo-vertical waveforms are generated, ALS_{FW} metrics may be extracted. In this manuscript we propose four new ALS_{FW} metrics (KURTOSIS, canopy distance (CD), canopy energy (CE), and the canopy energy ratio (CER)) and perform an exhaustive compilation of those proposed by previous recent studies [38–42]. All of them are available in the software tool. The ALS_{FW} metrics implemented can be divided into seven categories: height, energy, peaks, understory, percentiles, Gaussian decomposition, and others. Table 1 describes the different ALS_{FW} metrics classified by category.

Table 1. Description of ALS_{FW} metrics available in *WoLFeX* (adapted from Crespo-Peremarch et al. [38]).

Category	Name	Description	Units	Reference
Height	**WD**	Waveform distance	m	[41]
	ROUGH	Roughness of outermost canopy	m	
	HEIGHT Qn	Proportion of energy at the nth elevation quarter	-	[40]
Energy	**RWE**	Return waveform energy	DN (Digital Number)	[41]
	MAX E	Maximum energy	DN	[40]
	VARIANCE	Variance of energy	DN^2	
	SKEWNESS	Skewness of energy	-	
	ENERGY Qn	Proportion of energy at the nth energy quarter	-	
	KURTOSIS	Kurtosis of energy	-	This study
Peaks	**NP**	Number of peaks	-	[41]
	START PEAK	Distance between the beginning of the waveform and the height of MAX E	m	[40]
	PEAK END	Distance between the height of MAX E and the ground	m	
Understory	**HFEV**	Height of the first empty voxel	m	[38]
	HFEVT	Height of the first empty voxel from a given thresholds	m	
	EFEV	Energy from the ground to the first empty voxel	DN	
	nEFEV	Energy from the ground to the first empty voxel divided by RWE	-	
	FVU	Number of filled voxels at the understory	-	
	NFVU	Number of filled voxels at the understory divided by the total number of voxels	-	
Percentiles	**Hn**	Height at the nth percentiles of energy	m	[39]

Table 1. *Cont.*

Category	Name	Description	Units	Reference
Gaussian Decomposition	**N GS**	Number of Gaussian curves in the waveform	-	[40]
	N GS STARTPEAK	Number of Gaussian curves between the beginning of the waveform and the height of the boundary	-	
	N GS ENDPEAK	Number of Gaussian curves between the height of the boundary and the ground	-	
	GE	Ground energy extracted from the ground Gaussian curve	DN	[42]
	GRR	Ground return ratio: GE divided by RWE	-	
	CHn	Elevation of the nth quarter of energy, excluding the ground Gaussian curve	m	
	Rn	CHn divided by WD	-	
	AGS	Average Gaussian curve slope	-	
	SGS	Standard deviation Gaussian curve slope	-	
	MSGS	Modified standard deviation Gaussian curve slope	-	
	BC	Bottom of canopy: elevation of the first canopy Gaussian curve	m	[38]
	BCD	Bottom of canopy distance: distance from the beginning of the waveform to BC	m	
	BCE	Bottom of canopy energy: energy from the beginning of the waveform to BC	DN	
	CD	Canopy distance: distance from the beginning of the waveform to the boundary between ground and canopy	m	This study
	CE	Canopy energy: energy excluding GE	DN	
	CER	Canopy energy ratio: CE divided by RWE	-	
Others	**HTMR**	Height/median ratio: HOME divided by WD	-	[41]
	VDR	Vertical distribution ratio: WD minus HOME divided by WD	-	
	FS	Front slope: vertical angle from the beginning of the waveform to the amplitude of the first peak	º (sexagesimal)	

The first of the new proposed metrics is the kurtosis of the waveform amplitudes. The others depend on the Gaussian decomposition and metrics and concepts previously developed by Zhang et al. [42] and Crespo-Peremarch et al. [38] (Figure 3). After applying the Gaussian decomposition to the waveform signal, and according to Zhang et al. [42], the ground curve is identified as the one with the highest amplitude located in the half of the waveform with the lowest heights. Next, the boundary between ground and canopy curves is defined as the height at the ground curve plus 1.5 times its standard deviation. In this way, CD is the distance between the beginning of the waveform and this

boundary; CE is the energy from the beginning of the waveform to the boundary; and CER is equal to CE normalized by the total energy of the waveform (i.e., return waveform energy, RWE).

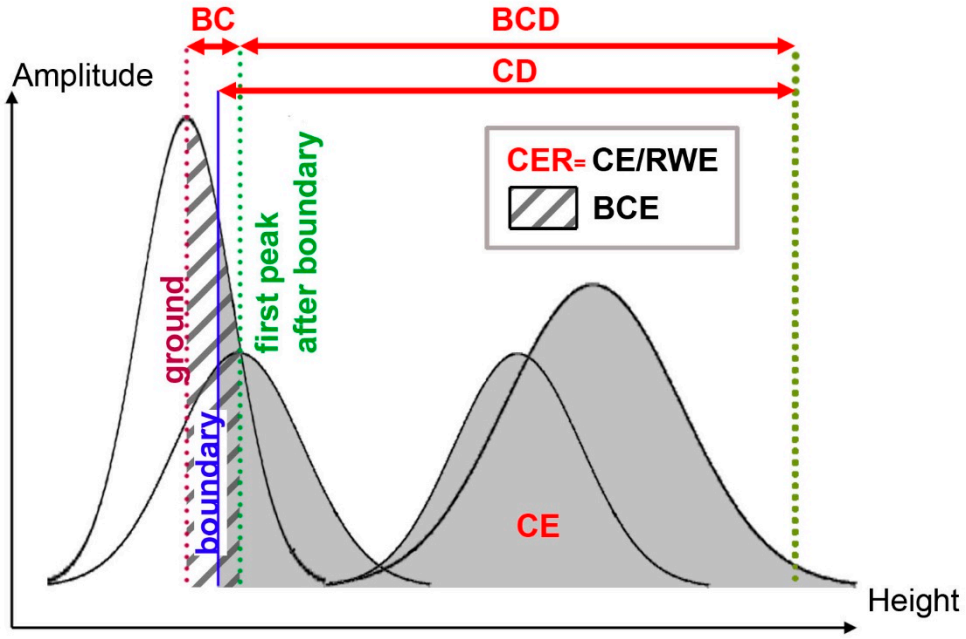

Figure 3. Representation of ALS_{FW} metrics BC: bottom of canopy, BCD: bottom of canopy distance, BCE: bottom of canopy energy, CD: canopy distance, CE: canopy energy, and CER: canopy energy ratio, which depends on RWE: return waveform energy.

As a result, each voxel column has a metric value assigned. Afterwards, the mean and the standard deviation of each ALS_{FW} metric contained in a given area or polygon (e.g., plot, segmented tree) are computed to obtain the output statistics at the object level.

3. Software Tool

The software tool *WoLFeX* is designed to perform all the processing steps described in the previous section, from the relative radiometric correction of ALS_{FW} data to the extraction of ALS_{FW} metrics for generating either regression or classification models, which can be further applied in larger study areas.

WoLFeX is divided into five sections (Figure 4): Inputs, Radiometric correction, Voxelization parameters, Metrics, and Execution. In the Inputs section, the user selects the ALS_{FW} data files, typically LAS files (version 1.3 and point format 4), the digital terrain model (DTM) for the height normalization, and a workspace to save the outputs. In order to process a smaller area, data may be clipped using the limits saved in shapefile format with a polygon geometry. In addition, if the clip area is representing objects such as plots or segmented trees, an id field from the shapefile must be selected in the Inputs section to identify the different processed objects in the output statistics. To apply a radiometric correction of the data, the trajectory files related to the LAS files must be selected. These trajectory files can be in *.txt or *.trj format and they are needed to compute the trajectory of each waveform. When the format is *.txt, the user should select the fields containing the GPS time, X, Y, and Z coordinates, and specify if there is a header in the text file. For both formats (*.txt and *.trj), the user should introduce a range of reference and a power n as described in Equation (1). On the other hand, *WoLFeX* also allows for filtering by scan angle intervals without selecting trajectory files. This option can be used to process a narrower range of scan angles to minimize the effect of a wide range of incidence angles on radiometric values. The third section allows for the selection of the *voxel size* and the *assignation value*. In the Metrics section, the user can select the specific ALS_{FW} metrics to compute. Lastly, the Execution section allows for the selection of the different processing steps that the

user wants to execute, as well as the output format (*.csv or *.tif) for the metrics. In addition, this is the section where the completed steps or possible error messages are printed after the execution of the process.

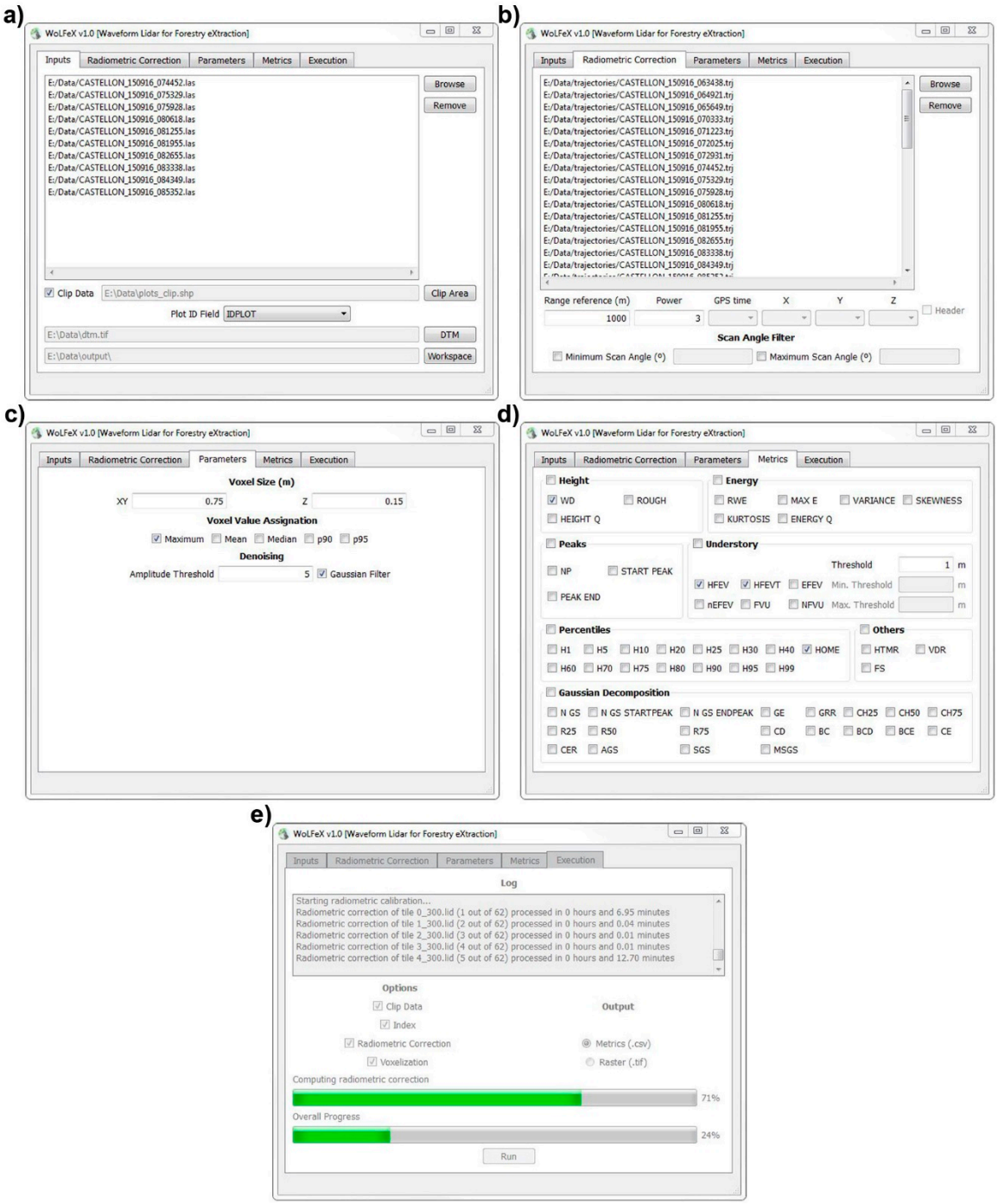

Figure 4. Graphic user interface of *WoLFeX* and the five different sections: (**a**) Inputs, (**b**) Radiometric correction, (**c**) Voxelization parameters, (**d**) Metrics, and (**e**) Execution.

4. Case of Study: Influence of Radiometric Correction and Forest Fuel Modelling

4.1. Materials and Methods

In this application example, we tested the effect of the relative radiometric correction of ALS_{FW} data on modelling forest fuel variables for different scan angle intervals using the described software tool *WoLFeX*. The study area was located in the Natural Park of Sierra de Espadán, 30 km west of the Mediterranean Sea in eastern Spain (Figure 5a). This area is dominated by Aleppo and maritime pines (*Pinus halepensis* and *Pinus pinaster*, respectively), and cork oak (*Quercus suber*), and it has a variable presence of Mediterranean shrub.

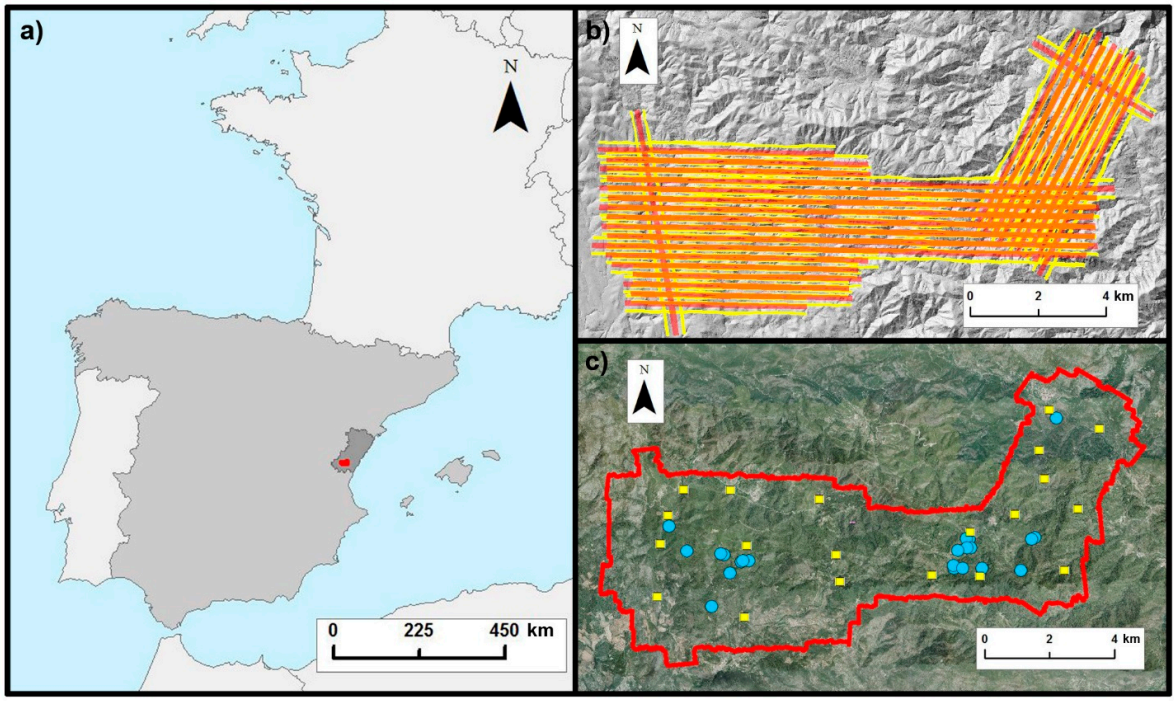

Figure 5. Maps of (**a**) the general location of the study area in Natural Park of Sierra de Espadán (Castellón, Spain), (**b**) flight stripes categorized by scan angle interval (0°–5° in orange and 15°–20° in yellow), and (**c**) sample locations (square samples for analyzing radiometric differences in RWE are represented in yellow, and circular samples for analyzing estimation of forest fuel variables are in blue).

ALS_{FW} data were acquired in September 2015 over an area of 7465 ha with altitudes ranging from 300 to 1000 m using a LiteMapper 6800 sensor. The flight altitude ranged between 600 and 820 m above ground level, with a scan angle of ±37° and a pulse frequency of 300 kHz, which yielded an average pulse density of 14 pulses·m^{-2} and an overlap of 55%–77% between contiguous flight stripes. Waveforms were registered in a variable number of bins (80–160–240 bins) with a gap of 0.15 m between bins and a footprint size of about 0.24 m. ALS_D data obtained from ALS_{FW} were used to generate the DTM of the study area.

Samples differed according to the test. Firstly, the influence of radiometric correction and scan angle on the values of ALS_{FW} metrics was analyzed in Test 1. To do this, 20 square samples of 75 m side (i.e., 5625 m^2) were selected in areas registered from different scan angles but with similar pulse densities. Secondly, 22 circular samples of 15 m radius (i.e., 706.86 m^2) were selected for Test 2, where the influence of the application of the radiometric correction and scan angle on modelling forest fuel variables was analyzed. Selected samples also needed to be registered from different scan angles and field data to estimate the forest fuel variables. The locations of the 42 samples for both tests are shown in Figure 5c. Ground-truth data collected from the 22 samples of Test 2 included diameter at breast height (DBH) from trees with a value greater or equal to 5 cm, height and canopy base height

from the seven trees with largest DBH, and tree species. Afterwards, allometric equations provided by Montero et al. [62] were used to compute the reference data of three forest fuel variables: canopy fuel load (CFL), canopy height (CH), and canopy base height (CBH).

ALS_{FW} metrics were extracted using *WoLFeX*, as described in Section 2.4, for the different combinations of scan angle intervals and relative radiometric corrections. Radiometric correction reduces the effect of energy loss of the pulse due to different factors such as range (i.e., distance from the sensor to the target), attenuation (because of penetration of pulse though vegetation), and angle of incidence (slope and target orientation) [60]. Given that the return waveform energy (RWE) metric represents the sum of the waveform amplitudes from the beginning of the canopy to the ground, it is highly sensitive to pulse energy losses along the trajectory. For this reason, and in order to avoid redundancies in the test, only this metric was selected as a good indicator to evaluate the influence of scan angle and radiometric correction on ALS_{FW} metrics. Hence, RWE metrics were extracted for the samples of Test 1, while all the metrics from Table 1 were extracted for the samples of Test 2. The two scan angle intervals tested were 0°–5° and 15°–20°, in an attempt to differentiate between nadir and off-nadir pulses, respectively. Four options were considered for the relative radiometric correction: uncorrected data, and corrected data varying the power n of Equation (1) (i.e., $n = 2$, $n = 3$, and $n = 4$). Hence, eight different data sets were computed (i.e., the combination of the two scan angle intervals and the four options for the relative radiometric correction) for the two sets of samples (i.e., Tests 1 and 2).

In Test 1, the mean values of RWE were computed for each sample at the different combinations. The RWE value variations were computed as the differences at sample level between two combinations. The combinations compared had the same radiometric correction but different scan angle interval (e.g., uncorrected data with a scan angle interval of 0°–5° and uncorrected data with a scan angle interval of 15°–20°). Additionally, the corrected data with a given scan angle interval were compared to their corresponding interval of uncorrected data (e.g., uncorrected data with a scan angle interval of 0°–5° and the corrected data with a power $n = 2$ and a scan angle interval of 0°–5°). Results were evaluated using the root-mean-square error (RMSE) of these differences and the normalized RMSE (nRMSE), computed as the RMSE divided by the range of RWE values in the sample.

4.2. Results and Discussion

Table 2 shows the RWE differences between the different scan angle intervals by means of RMSE and nRMSE. Results show that differences in RWE values between scan angle intervals decreased when relative radiometric correction was applied and as power (n) increased. For instance, uncorrected data had an RMSE of 262.29, while corrected data had a value of 117.41 and 93.25 for a power $n = 3$ and $n = 4$, respectively. This means that the influence of the scan angle on the metric value was smaller when using radiometrically corrected data, but it was not completely removed. On the other hand, results in Table 3 show that differences between uncorrected and corrected data increased as the power n increased, and the effect of the radiometric correction on the metrics was more obvious at small scan angle intervals. For instance, differences between corrected data with a power $n = 2$ and a scan angle interval of 0°–5° were equal to 183.86, while using the same scan angle interval and a power $n = 4$ differences were equal to 299.29. Moreover, using the same power n but a scan angle interval of 15°–20° resulted in differences of 90.74 and 164.43, respectively. This means that the larger the power n and the smaller the scan angle, the larger the correction that is applied to the uncorrected data. Analyzing Equation (1), this occurred in this study since the range of reference was larger than the rest of the ranges; otherwise, it would be the opposite.

Table 2. RWE differences between the different scan angle intervals (0°–5° and 15°–20°). RMSE: root-mean-square error; nRMSE: normalized RMSE.

Radiometrically Corrected Data	Power *n*	Differences between 0°–5° and 15°–20°	
		RMSE	nRMSE
No	-	262.29	15.40%
Yes	2	150.71	13.32%
Yes	3	117.41	11.21%
Yes	4	93.25	11.74%

Table 3. RWE differences between the radiometrically uncorrected and corrected data.

Scan Angle Interval	Power *n*	Differences between Uncorrected and Corrected Data	
		RMSE	nRMSE
0°–5°	2	183.86	9.98%
15°–20°		90.74	5.39%
0°–5°	3	248.31	13.48%
15°–20°		128.57	7.63%
0°–5°	4	299.29	16.25%
15°–20°		164.43	9.76%

For the Test 2, the mean and the standard deviation of all the ALS_{FW} metrics described in Section 2.4 were computed at the sample level using *WoLFeX*. As a result, the software tool provided a *.csv file that was used as the input file in statistical software. All possible combinations of linear regression models with a maximum of three metrics were computed, finally selecting the model with the minimum Akaike information criterion (AIC) [63]. Among the selected ALS_{FW} metrics, those proposed in the present manuscript (i.e., KURTOSIS, CD, CE, and CER) were among the most selected, and therefore they had an influence on estimating forest fuel variables. For instance, KURTOSIS was selected to estimate CFL and CBH, CD for CH, and CE for CBH. Afterwards, a model was obtained for each of the three forest fuel variables (i.e., CFL, CH, and CBH), each combination of scan angle interval (i.e., 0°–5° and 15°–20°), and each radiometric correction type (i.e., uncorrected and corrected data with a power n = 2, n = 3, and n = 4). The linear regression models were evaluated using leave-one-out cross-validation and computing the adjusted coefficient of determination (R^2), RMSE, nRMSE, and coefficient of variation (CV). Table 4 shows the prediction of forest fuel variables (i.e., CFL, CH, and CBH) using varied scan angle interval and radiometric correction. The prediction of CFL was considerably improved when a radiometric correction was applied with a higher power n for both scan angle intervals, varying R^2 from 0.62 to 0.79 and from 0.68 to 0.85 for scan angle intervals of 0°–5° and 15°–20°, respectively. Additionally, R^2 also increased as the scan angle interval increased, except for a power n = 2. Prediction results of CH were slightly improved when a radiometric correction was applied, varying from 0.89 to 0.93 and from 0.91 to 0.92 for a scan angle interval of 0°–5° and 15°–20°, respectively. However, CBH prediction results did not improve, or even slightly worsened, when a radiometric correction was applied. In this case, differences were also smaller compared to CFL, and as in the CH predictions, results were similar for a scan angle interval of 15°–20°. The test shows that the influence of the radiometric correction was smaller in predicting height variables such as CH and CBH than in predicting mass-related variables such as CFL. Height variables are fixed at a specific point on the waveform, usually a maximum or minimum, while mass-related variables are described using the complete waveform profile. Therefore, the latter are more subjected to radiometric values. Additionally, the difference between uncorrected and corrected data for the three forest fuel variables was smaller when the scan angle interval was 15°–20° than when it was 0°–5°. Previous analyses [64] found that parameters corrected by radiometric correction such as flying altitude and

incidence angle have an influence on estimates of biophysical vegetation properties (i.e., tree height, crown width, fractional cover, and leaf area index). However, the influence of scan angle was not as apparent here, probably due to the use of small scan angles. Additionally, other studies also mentioned the radiometric calibration as a key step in using backscattered measurements to estimate geophysical vegetation properties or similar analyses [49,51].

Table 4. Prediction of forest fuel variables (i.e., CFL, CH, and CBH) using varied scan angle interval and radiometric correction.

Forest Fuel Variable	Scan Angle Interval	Radiometrically Corrected Data	Power *n*	R^2	RMSE	nRMSE	CV
CFL	0°–5°	No	-	0.62	4.61 [1]	0.15	0.20
		Yes	2	0.75	3.67 [1]	0.12	0.16
		Yes	3	0.77	3.55 [1]	0.11	0.15
		Yes	4	0.79	3.37 [1]	0.11	0.15
	15°–20°	No	-	0.68	4.13 [1]	0.13	0.18
		Yes	2	0.72	3.84 [1]	0.12	0.17
		Yes	3	0.83	3.04 [1]	0.10	0.13
		Yes	4	0.85	2.86 [1]	0.09	0.12
CH	0°–5°	No	-	0.89	1.09 [2]	0.08	0.08
		Yes	2	0.88	1.18 [2]	0.09	0.09
		Yes	3	0.93	0.89 [2]	0.07	0.07
		Yes	4	0.86	1.25 [2]	0.10	0.09
	15°–20°	No	-	0.91	1.02 [2]	0.08	0.08
		Yes	2	0.90	1.05 [2]	0.08	0.08
		Yes	3	0.91	0.99 [2]	0.08	0.07
		Yes	4	0.92	0.95 [2]	0.07	0.07
CBH	0°–5°	No	-	0.94	0.68 [2]	0.06	0.11
		Yes	2	0.93	0.73 [2]	0.06	0.12
		Yes	3	0.92	0.83 [2]	0.07	0.14
		Yes	4	0.89	0.89 [2]	0.07	0.15
	15°–20°	No	-	0.96	0.56 [2]	0.05	0.09
		Yes	2	0.92	0.74 [2]	0.06	0.12
		Yes	3	0.95	0.61 [2]	0.05	0.10
		Yes	4	0.95	0.59 [2]	0.05	0.10

[1] $Mg \cdot ha^{-1}$; [2] m.

5. Conclusions

In this manuscript we presented and described a software tool named *WoLFeX*, designed to process ALS_{FW} data, which includes a wide range of new and previously proposed ALS_{FW} metrics. We assessed the influence of radiometric correction on ALS_{FW} metrics and on estimates of forest fuel variables through *WoLFeX*.

This tool allows for clipping, radiometrically correcting, and voxelizing the original ALS_{FW} waveforms, creating pseudo-vertical waveforms, and extracting an exhaustive set of object-oriented metrics. These metrics are saved into a *.csv file that can be used as an input file for generating either regression or classification models, such as forest fuel variables or fuel types, respectively. Among these metrics, those related to the understory vegetation are the most remarkable, since they have not been considered by other processing tools so far, and they allow for the location and quantification of understory vegetation, which is a key parameter for the characterization of fire behavior in Mediterranean forests. Processing ALS_{FW} is more challenging than ALS_D, since it registers the complete return of the signal, and therefore it allows for a better detection of the lower strata.

From the case of study of *WoLFeX* software, different models of forest fuel variables (CFL, CH, and CBH) were generated, varying processing parameters related to radiometric correction and scan angle interval of ALS_{FW} data acquisition. These tests showed that differences in metric values measured

from nadir and off-nadir were reduced when a relative radiometric correction was applied. The improvement of the models obtained when the relative radiometric correction of the data was applied was noteworthy—from R^2 = 0.62 up to R^2 = 0.79 in the case of CFL. However, height variables (i.e., CH and CBH) were less strongly influenced by a relative radiometric correction, presenting only subtle differences.

The software *WoLFeX*, freely available for download at (http://cgat.webs.upv.es/software/), is an alternative for processing ALS_{FW} data in an integrated manner. It includes the relative radiometric correction of the data, which plays an important role in reducing radiometric differences between different scan angles and may be essential for estimating some forest fuel variables. It also extracts multiple new and previously proposed metrics to generate models that characterize forest structure. Among these metrics, the most remarkable are those related to understory vegetation, due to the potential of ALS_{FW} to register the complete vertical forest structure. This opens a wide range of applications in environmental sciences, forestry, and fire ecology.

Author Contributions: Conceptualization, P.C.-P. and L.A.R.; Formal Analysis, P.C.-P. and L.A.R.; Funding Acquisition, L.A.R.; Investigation, P.C.-P. and L.A.R.; Methodology, P.C.-P. and L.A.R.; Project Administration, L.A.R.; Software, P.C.-P.; Supervision, L.A.R.; Writing—Original Draft, P.C.-P. and L.A.R.; Writing—Review and Editing, P.C.-P. and L.A.R. All authors have read and agreed to the published version of the manuscript.

Funding: This research was funded by the Spanish Ministerio de Economía y Competitividad and FEDER, in the framework of the projects ForeStructure (CGL2013-46387-C2-1-R) and FIRMACARTO (CGL2016-80705-R).

Conflicts of Interest: The authors declare no conflict of interest.

References

1. González-Ferreiro, E.; Diéguez-Aranda, U.; Miranda, D. Estimation of stand variables in Pinus radiata D. Don plantations using different LiDAR pulse densities. *Forestry* **2012**, *85*, 281–292. [CrossRef]
2. Kankare, V.; Holopainen, M.; Vastaranta, M.; Puttonen, E.; Yu, X.; Hyyppä, J.; Vaaja, M.; Hyyppä, H.; Alho, P. Individual tree biomass estimation using terrestrial laser scanning. *ISPRS J. Photogramm. Remote Sens.* **2013**, *75*, 64–75. [CrossRef]
3. García, M.; Riaño, D.; Chuvieco, E.; Danson, F.M. Estimating biomass carbon stocks for a Mediterranean forest in central Spain using LiDAR height and intensity data. *Remote Sens. Environ.* **2010**, *114*, 816–830. [CrossRef]
4. Hudak, A.T.; Strand, E.K.; Vierling, L.A.; Byrne, J.C.; Eitel, J.U.H.; Martinuzzi, S.; Falkowski, M.J. Quantifying aboveground forest carbon pools and fluxes from repeat LiDAR surveys. *Remote Sens. Environ.* **2012**, *123*, 25–40. [CrossRef]
5. Vogeler, J.C.; Cohen, W.B. A review of the role of active remote sensing and data fusion for characterizing forest in wildlife habitat models. *Revista de Teledetección* **2016**, 1–14. [CrossRef]
6. Guo, X.; Coops, N.C.; Tompalski, P.; Nielsen, S.E.; Bater, C.W.; John Stadt, J. Regional mapping of vegetation structure for biodiversity monitoring using airborne lidar data. *Ecol. Inform.* **2017**, *38*, 50–61. [CrossRef]
7. Lim, K.; Treitz, P.; Wulder, M.A.; St-Onge, B.; Flood, M. LiDAR remote sensing of forest structure. *Prog. Phys. Geogr.* **2003**, *27*, 88–106. [CrossRef]
8. Côté, J.-F.; Fournier, R.A.; Egli, R. An architectural model of trees to estimate forest structural attributes using terrestrial LiDAR. *Environ. Model. Softw.* **2011**, *26*, 761–777. [CrossRef]
9. Béland, M.; Widlowski, J.-L.; Fournier, R.A. A model for deriving voxel-level tree leaf area density estimates from ground-based LiDAR. *Environ. Model. Softw.* **2014**, *51*, 184–189. [CrossRef]
10. Li, W.; Guo, Q.; Jakubowski, M.K.; Kelly, M. A new method for segmenting individual rrees from the lidar point cloud. *Photogramm. Eng. Remote Sens.* **2012**, *78*, 75–84. [CrossRef]
11. Dalponte, M.; Coomes, D.A. Tree-centric mapping of forest carbon density from airborne laser scanning and hyperspectral data. *Methods Ecol. Evol.* **2016**, *7*, 1236–1245. [CrossRef] [PubMed]
12. Means, J.E.; Acker, S.A.; Fitt, B.J.; Renslow, M.; Emerson, L.; Hendrix, C.J. Predicting forest stand characteristics with airborne scanning lidar. *Photogramm. Eng. Remote Sens.* **2000**, *66*, 1367–1372. [CrossRef]

13. Bottalico, F.; Chirici, G.; Giannini, R.; Mele, S.; Mura, M.; Puxeddu, M.; McRoberts, R.E.; Valbuena, R.; Travaglini, D. Modeling Mediterranean forest structure using airborne laser scanning data. *Int. J. Appl. Earth Obs. Geoinf.* **2017**, *57*, 145–153. [CrossRef]
14. Lindberg, E.; Hollaus, M. Comparison of methods for estimation of stem volume, stem number and basal area from airborne laser scanning data in a hemi-boreal forest. *Remote Sens.* **2012**, *4*, 1004–1023. [CrossRef]
15. Luther, J.E.; Skinner, R.; Fournier, R.A.; van Lier, O.R.; Bowers, W.W.; Cote, J.-F.; Hopkinson, C.; Moulton, T. Predicting wood quantity and quality attributes of balsam fir and black spruce using airborne laser scanner data. *Forestry* **2014**, *87*, 313–326. [CrossRef]
16. Hyyppä, J.; Yu, X.; Hyyppä, H.; Vastaranta, M.; Holopainen, M.; Kukko, A.; Kaartinen, H.; Jaakkola, A.; Vaaja, M.; Koskinen, J.; et al. Advances in forest inventory using airborne laser scanning. *Remote Sens.* **2012**, *4*, 1190–1207. [CrossRef]
17. Kankare, V.; Vastaranta, M.; Holopainen, M.; Räty, M.; Yu, X.; Hyyppä, J.; Hyyppä, H.; Alho, P.; Viitala, R. Retrieval of forest aboveground biomass and stem volume with airborne scanning LiDAR. *Remote Sens.* **2013**, *5*, 2257–2274. [CrossRef]
18. Guerra-Hernández, J.; Tomé, M.; González-Ferreiro, E. Using low density LiDAR data to map Mediterranean forest characteristics by means of an area-based approach and height threshold analysis. *Revista de Teledetección* **2016**, 103–117. [CrossRef]
19. Hevia, A.; Álvarez-González, J.G.; Ruiz-Fernández, E.; Prendes, C.; Ruiz-González, A.D.; Majada, J.; González-Ferreiro, E. Modelling canopy fuel and forest stand variables and characterizing the influence of thinning in the stand structure using airborne LiDAR. *Revista de Teledetección* **2016**, 41–55. [CrossRef]
20. Morsdorf, F.; Kötz, B.; Meier, E.; Itten, K.I.; Allgöwer, B. Estimation of LAI and fractional cover from small footprint airborne laser scanning data based on gap fraction. *Remote Sens. Environ.* **2006**, *104*, 50–61. [CrossRef]
21. Sasaki, T.; Imanishi, J.; Ioki, K.; Song, Y.; Morimoto, Y. Estimation of leaf area index and gap fraction in two broad-leaved forests by using small-footprint airborne LiDAR. *Landsc. Ecol. Eng.* **2016**, *12*, 117–127. [CrossRef]
22. Suárez, J.C.; Ontiveros, C.; Smith, S.; Snape, S. Use of airborne LiDAR and aerial photography in the estimation of individual tree heights in forestry. *Comput. Geosci.* **2005**, *31*, 253–262. [CrossRef]
23. Andersen, H.-E.; McGaughey, R.J.; Reutebuch, S.E. Estimating forest canopy fuel parameters using LIDAR data. *Remote Sens. Environ.* **2005**, *94*, 441–449. [CrossRef]
24. Dalponte, M.; Bruzzone, L.; Gianelle, D. Tree species classification in the Southern Alps based on the fusion of very high geometrical resolution multispectral/hyperspectral images and LiDAR data. *Remote Sens. Environ.* **2012**, *123*, 258–270. [CrossRef]
25. Matsuki, T.; Yokoya, N.; Iwasaki, A. Hyperspectral tree species classification of Japanese complex mixed forest with the aid of lidar data. *IEEE J. Sel. Top. Appl. Earth Obs. Remote Sens.* **2015**, *8*, 2177–2187. [CrossRef]
26. García, M.; Riaño, D.; Chuvieco, E.; Salas, J.; Danson, F.M. Multispectral and LiDAR data fusion for fuel type mapping using Support Vector Machine and decision rules. *Remote Sens. Environ.* **2011**, *115*, 1369–1379. [CrossRef]
27. Crespo-Peremarch, P.; Ruiz, L.A. Influence of LiDAR of Full-Waveform density and voxel size on forest influence of LiDAR Full-Waveform density and voxel size on forest stand estimates. In Proceedings of the International Geoscience and Remote Sensing Symposium, Valencia, Spain, 22–27 July 2018; IEEE: Pìscataway, NJ, USA. [CrossRef]
28. García, M.; Danson, F.M.; Riaño, D.; Chuvieco, E.; Ramirez, F.A.; Bandugula, V. Terrestrial laser scanning to estimate plot-level forest canopy fuel properties. *Int. J. Appl. Earth Obs. Geoinf.* **2011**, *13*, 636–645. [CrossRef]
29. Mallet, C.; Bretar, F. Full-waveform topographic lidar: State-of-the-art. *ISPRS J. Photogramm. Remote Sens.* **2009**, *64*, 1–16. [CrossRef]
30. Hermosilla, T.; Ruiz, L.A.; Kazakova, A.N.; Coops, N.C.; Moskal, L.M. Estimation of forest structure and canopy fuel parameters from small-footprint full-waveform LiDAR data. *Int. J. Wildland Fire* **2014**, *23*, 224–233. [CrossRef]
31. Cao, L.; Coops, N.C.; Hermosilla, T.; Innes, J.; Dai, J.; She, G. Using small-footprint discrete and full-waveform airborne LiDAR metrics to estimate total biomass and biomass components in subtropical forests. *Remote Sens.* **2014**, *6*, 7110–7135. [CrossRef]

32. Reitberger, J.; Schnörr, C.; Krzystek, P.; Stilla, U. 3D segmentation of single trees exploiting full waveform LIDAR data. *ISPRS J. Photogramm. Remote Sens.* **2009**, *64*, 561–574. [CrossRef]
33. Heinzel, J.; Koch, B. Exploring full-waveform LiDAR parameters for tree species classification. *Int. J. Appl. Earth Obs. Geoinf.* **2011**, *13*, 152–160. [CrossRef]
34. Cao, L.; Coops, N.C.; Innes, J.L.; Dai, J.; Ruan, H.; She, G. Tree species classification in subtropical forests using small-footprint full-waveform LiDAR data. *Int. J. Appl. Earth Obs. Geoinf.* **2016**, *49*, 39–51. [CrossRef]
35. Ruiz, L.A.; Hermosilla, T.; Mauro, F.; Godino, M. Analysis of the influence of plot size and LiDAR density on forest structure attribute estimates. *Forests* **2014**, *5*, 936–951. [CrossRef]
36. Crespo-Peremarch, P.; Ruiz, L.Á.; Balaguer-Beser, Á. A comparative study of regression methods to predict forest structure and canopy fuel variables from LiDAR full-waveform data. *Revista de Teledetección* **2016**, 27–40. [CrossRef]
37. Hancock, S.; Anderson, K.; Disney, M.; Gaston, K.J. Measurement of fine-spatial-resolution 3D vegetation structure with airborne waveform lidar: Calibration and validation with voxelised terrestrial lidar. *Remote Sens. Environ.* **2017**, *188*, 37–50. [CrossRef]
38. Crespo-Peremarch, P.; Tompalski, P.; Coops, N.C.; Ruiz, L.Á. Characterizing understory vegetation in Mediterranean forests using full-waveform airborne laser scanning data. *Remote Sens. Environ.* **2018**, *217*, 400–413. [CrossRef]
39. Kimes, D.S.; Ranson, K.J.; Sun, G.; Blair, J.B. Predicting lidar measured forest vertical structure from multi-angle spectral data. *Remote Sens. Environ.* **2006**, *100*, 503–511. [CrossRef]
40. Duncanson, L.I.; Niemann, K.O.; Wulder, M.A. Estimating forest canopy height and terrain relief from GLAS waveform metrics. *Remote Sens. Environ.* **2010**, *114*, 138–154. [CrossRef]
41. Duong, V.H. Processing and Application of ICEsat Large Footprint Full Waveform Laser Range Data. Ph.D. Thesis, University of Technology, Delft, The Netherlands, 8 June 2010.
42. Zhang, J.; de Gier, A.; Xing, Y.; Sohn, G. Full Waveform-based analysis for forest type information derivation from large footprint spaceborne lidar data. *Photogramm. Eng. Remote Sens.* **2011**, *77*, 281–290. [CrossRef]
43. Yu, X.; Litkey, P.; Hyyppä, J.; Holopainen, M.; Vastaranta, M. Assessment of low density full-waveform airborne laser scanning for individual tree detection and tree species classification. *Forests* **2014**, *5*, 1011–1031. [CrossRef]
44. Ruiz, L.Á.; Recio, J.A.; Crespo-Peremarch, P.; Sapena, M. An object-based approach for mapping forest structural types based on low-density LiDAR and multispectral imagery. *Geocarto Int.* **2018**, *33*, 443–457. [CrossRef]
45. Crespo-Peremarch, P.; Ruiz, L.Á.; Balaguer-Beser, Á.; Estornell, J. Analyzing the role of pulse density and voxelization parameters on full-waveform LiDAR-derived metrics. *ISPRS J. Photogramm. Remote Sens.* **2018**, *146*, 453–464. [CrossRef]
46. Xu, K.; Gong, Y.; Fang, S.; Wang, K.; Lin, Z.; Wang, F. Radiometric calibration of UAV remote sensing image with spectral angle constraint. *Remote Sens.* **2019**, *11*, 1291. [CrossRef]
47. Mafanya, M.; Tsele, P.; Botai, J.O.; Manyama, P.; Chirima, G.J.; Monate, T. Radiometric calibration framework for ultra-high-resolution UAV-derived orthomosaics for large-scale mapping of invasive alien plants in semi-arid woodlands: Harrisia pomanensis as a case study. *Int. J. Remote Sens.* **2018**, *39*, 5119–5140. [CrossRef]
48. Chander, G.; Markham, B.L.; Helder, D.L. Summary of current radiometric calibration coefficients for Landsat MSS, TM, ETM+, and EO-1 ALI sensors. *Remote Sens. Environ.* **2009**, *113*, 893–903. [CrossRef]
49. Wagner, W. Radiometric calibration of small-footprint full-waveform airborne laser scanner measurements: Basic physical concepts. *ISPRS J. Photogramm. Remote Sens.* **2010**, *65*, 505–513. [CrossRef]
50. Briese, C.; Pfennigbauer, M.; Lehner, H.; Ullrich, A.; Wagner, W.; Pfeifer, N. Radiometric calibration of multi-wavelength airborne laser scanning data. *ISPRS Ann. Photogramm. Remote Sens. Spat. Inf. Sci.* **2012**, *I-7*, 335–340. [CrossRef]
51. Sevara, C.; Wieser, M.; Doneus, M.; Pfeifer, N. Relative radiometric calibration of airborne LiDAR data for archaeological applications. *Remote Sens.* **2019**, *11*, 945. [CrossRef]
52. McGaughey, R.J. *FUSION/LDV: Software for LiDAR Data Analysis and Visualization*; Department of Agriculture, Forest Service, Pacific Northwest Research Station: Seattle, WA, USA, 2014.
53. Isenburg, M. *LAStools*; Rapidlasso GmbH: Gilching, Germany, 2017.

54. Roussel, J.R.; Auty, D. lidR: Airborne LiDAR Data Manipulation and Visualization for Forestry Applications. 2017.
55. Zhou, T.; Popescu, S. Waveformlidar: An R package for waveform LiDAR processing and analysis. *Remote Sens.* **2019**, *11*, 2552. [CrossRef]
56. Miltiadou, M.; Grant, M.; Campbell, N.D.; Warren, M.; Clewley, D.; Hadjimitsis, D. Open source software DASOS: Efficient accumulation, analysis, and visualisation of full-waveform lidar. In Proceedings of the 7th International Conference on Remote Sensing and Geoinformation of the Environment (RSCy2019), Paphos, Cyprus, 18–21 March 2019; p. 68.
57. Pfeifer, N.; Mandlburger, G.; Otepka, J.; Karel, W. OPALS—A framework for Airborne Laser Scanning data analysis. *Comput. Environ. Urban Syst.* **2014**, *45*, 125–136. [CrossRef]
58. Isenburg, M. *PulseWaves: An Open, Vendor-Neutral, Stand-Alone, LAS-Compatible Full Waveform LiDAR Standard*; Rapidlasso GmbH: Gilching, Germany; Available online: https://rapidlasso.com/pulsewaves (accessed on 21 November 2019).
59. Hermosilla, T.; Coops, N.C.; Ruiz, L.A.; Moskal, L.M. Deriving pseudo-vertical waveforms from small-footprint full-waveform LiDAR data. *Remote Sens. Lett.* **2014**, *5*, 332–341. [CrossRef]
60. Kashani, A.G.; Olsen, M.J.; Parrish, C.E.; Wilson, N. A review of LiDAR radiometric processing: From ad hoc intensity correction to rigorous radiometric calibration. *Sensors* **2015**, *15*, 28099–28128. [CrossRef] [PubMed]
61. Lefsky, M.A.; Harding, D.J.; Keller, M.; Cohen, W.B.; Carabajal, C.C.; Del Bom Espirito-Santo, F.; Hunter, M.O.; de Oliveira, R., Jr. Estimates of forest canopy height and aboveground biomass using ICESat. *Geophys. Res. Lett.* **2005**, *32*. [CrossRef]
62. Montero, G.; Ruiz-Peinado, R.; Muñoz, M. *Producción de Biomasa y Fijación de CO2 Por Los Bosques Españoles*; Instituto Nacional de Investigación y Tecnología Agraria y Alimentaria, Ministerio de Educación y Ciencia: Madrid, Spain, 2005.
63. Akaike, H. Information theory and an extension of the maximum likelihood principle. In Proceedings of the 2nd International Symposium on Information Theory, Akademiai Kiado, Budapest, Hungary, 2–8 September 1971.
64. Morsdorf, F.; Frey, O.; Meier, E.; Itten, K.I.; Allgöwer, B. Assessment of the influence of flying altitude and scan angle on biophysical vegetation products derived from airborne laser scanning. *Int. J. Remote Sens.* **2008**, *29*, 1387–1406. [CrossRef]